Crystal Growth

Deutsche Ausgabe: DOI: 10.1002/ange.201602907
Internationale Ausgabe: DOI: 10.1002/anie.201602907

Minimization of Surface Energies and Ripening Outcompete Template Effects in the Surface Growth of Metal–Organic Frameworks

*Xiu-Jun Yu, Jin-Liang Zhuang, Julian Scherr, Tarek Abu-Husein, and Andreas Terfort**

Abstract: *As well-oriented, surface-bound metal–organic frameworks become the centerpiece of many new applications, a profound understanding of their growth mode becomes necessary. This work shows that the currently favored model of surface templating is in fact a special case valid only for systems with a more or less cubic crystal shape, while in less symmetric systems crystal ripening and minimization of surface energies dominate the growth process.*

The immense potential of surface-attached metal–organic frameworks (SURMOFs) to serve as functional materials for numerous applications, including chemical sensors, optoelectronics, electronic devices, and membranes, have attracted significant interest throughout the scientific community.[1–8] Several methods[9–14] for the formation of SURMOFs have been developed, which often permit adjusting film thickness, homogeneity, morphology, crystallographic orientation, lateral position, and/or surface roughness. Of these, a method called layer-by-layer (LbL) growth exhibits striking advantages in controlling the mentioned features, which can be crucial for MOF-based device applications.[15–19] It is generally accepted that, independent of the deposition method, the key for the growth of homogeneous and highly oriented SURMOFs is the suitable adjustment of the surface chemistry, as it determines the interactions between the MOF structure and the surface. A very convenient method to control the surface chemistry is the use of self-assembled monolayers (SAMs), which can be tailored to expose a variety of functional groups.[20–24] In the case of coordinating head groups (e.g. -COOH or $-NH_2$), these can directly interact with the metal ions at the interface with the SURMOF, which does not only contribute to a tight binding, but also opens opportunities to control the orientation of the growing SURMOF crystallites.[13,22,25,26]

Two classes of MOFs, which both are based on secondary building units (SBUs) comprising dinuclear tetracarboxylate clusters $[M_2(O_2CR)_4]$ having the so-called paddle-wheel symmetry, have been successfully deposited in the form of highly defined SURMOFs. First, the cubic HKUST-1 MOF (Cu_3btc_2; btc = benzene-1,3,5-tricarboxylate) and its derivatives,[13,27] and second, the tetragonal, layered MOFs of the general formula $[M_2L_2P]$, where $M = Cu^{2+}$ or Zn^{2+}, L = a rigid, linear dicarboxylate linker, and P = an optional diamine pillar.[22,26,28,29] While the first class of MOFs can be formed very reliably and thus has turned out to be a very robust test system, the pillared-layer system shows a larger structural variability, and thus a broader range of potential applications, because of the basically independent choice of L and P. A set of rules has been developed to predict the surface growth of these MOFs. While for the cubic HKUST-1 systems mostly the density of coordinating groups at the surface seems to determine the SURMOF's orientation,[30] in the tetragonal pillared-layer system the nature of the surface-exposed ligands is of major importance. Thus, monodentate functional groups (e.g. -OH or pyridyl), which coordinate at the apical position of the paddle-wheel SBUs, usually induce SURMOF growth in the [001] direction, while bidentate ones (typically $-COO^-$) promote a growth in either the [100] or the [010] direction, depending on the exact symmetry of the MOF system.[13,22,31] In extension of these intuitive rules, a recent in-depth study could show that in fact an interplay of surface functionalities, deposition temperature, and first layer order determines the orientation and crystal quality of SURMOFs.[31] These findings opened the possibility to obtain high quality pillared layer SURMOFs by correctly adjusting all the relevant parameters.

In our efforts to extend the scope of available SURMOF systems, we decided to turn to a new series of $[M_2L_2P]$-type MOFs. These MOFs are based on V-shaped ligands, such as isophthalate derivatives or 4,4′-sulfonyldibenzoate (sdb),[32,33] which together with the metal SBUs form one-dimensional coordination polymers, which become expanded to two-dimensional (2D) sheets by the pillar ligands. Often a second network can interdigitate into the structure, thus reinforcing the 2D sheets. The sheets are held together mostly by van der Waals forces and, as in the case of the sdb ligand, by dipolar interactions between the highly polar sulfone groups (see Figure S2 in the Supporting Information for structural details). These structural features inherently lower the symmetry of the systems, but result in unique guest-molecule adsorption properties arising from the flexible nature of their 2D layer structure.[32] Attempts to grow well-defined SURMOFs of such systems have failed so far.[34]

Based on our previous studies on the interplay between surface chemistry and deposition temperature, we set out to deposit the orthorhombic $[Cu_2(sdb)_2(bipy)]$ MOF onto SAMs of either 4′-(mercaptomethyl)terphenyl-4-carboxylic acid

[*] X. J. Yu, J. Scherr, T. Abu-Husein, Prof. A. Terfort
Department of Biochemistry, Chemistry, and Pharmacy
University of Frankfurt
Max-von-Laue-Strasse 7, 60438 Frankfurt/M. (Germany)
E-mail: aterfort@chemie.uni-frankfurt.de
Dr. J. L. Zhuang
School of Chemistry and Materials, Guizhou Normal University
Guiyang, 550001 (P.R. China)
and
State Key Laboratory of Physical Chemistry of Solid Surfaces
Xiamen University, Xiamen, 361005 (P.R. China)

Supporting information for this article can be found under: http://dx.doi.org/10.1002/anie.201602907.

(MTCA) or 4′-(mercaptomethyl)-4-(4-pyridyl)biphenyl (PPP1) on gold.[31] After about 40 deposition cycles, only two crystallographic orientations could be found in the out-of-plane surface X-ray-diffractometry (SXRD; Figure 1a), namely [001] and [010], as could be expected from the templating chemistry (see Figure S3). It was nevertheless completely unanticipated that the orientation of the SURMOF exclusively depended on the deposition temperature, regardless of the surface chemistry (Figure 1b). Phenomenologically, this behavior can be divided into three distinct temperature regimes: At low temperatures (up to 35 °C), the crystals are exclusively [010] oriented. In the middle-temperature regime (40 °C to approx. 55 °C), [001] orientation predominates, while at higher temperatures the admixture of [010] orientated material increases again. The different orientations also become visible in the scanning-electron micrographs (SEM), where the plate-like crystals can be seen standing up (low temperatures, Figure 1c), lying down (medium temperatures, Figure 1d), or mixed (high temperatures, Figure 1e). In the latter case, the shape of the crystals has also changed to a chubbier, more rodlike form.

To understand this unexpected behavior, we applied surface IR spectroscopy to the deposits after one and 40 deposition cycles. This powerful technique permits the determination of the orientation of functional groups in the vicinity of metal surfaces because of the directed dipolar shielding/enhancement of the vibrational excitations (surface selection rules[35]). We used the asymmetric and the symmetric carboxylate vibrations at 1650 cm^{-1} and 1420 cm^{-1} to learn about the orientation of the SURMOF during its growth. The spectra of the fully grown material (40 cycles) reproduce the orientational behavior found by SXRD (Figure 1b, solid symbols). Surprisingly, the orientation of the material after one cycle shows a completely inverted behavior (Figure 2): at low temperature, the [001] orientation is preferred, while at higher temperatures the SURMOF layer is predominantly [010] oriented. The transition temperature is again, as in the

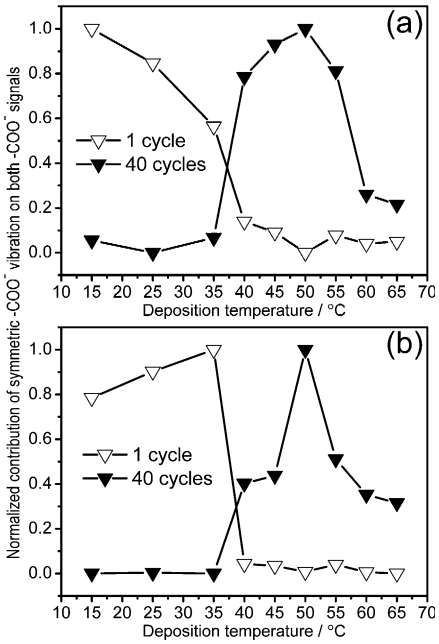

Figure 2. IRRAS data for the films on PPP1 (a) and MTCA (b) after one and 40 cycles. While the data for the thicker films basically reproduce the SXRD data, both systems show a distinct reorientation in both temperature regimes.

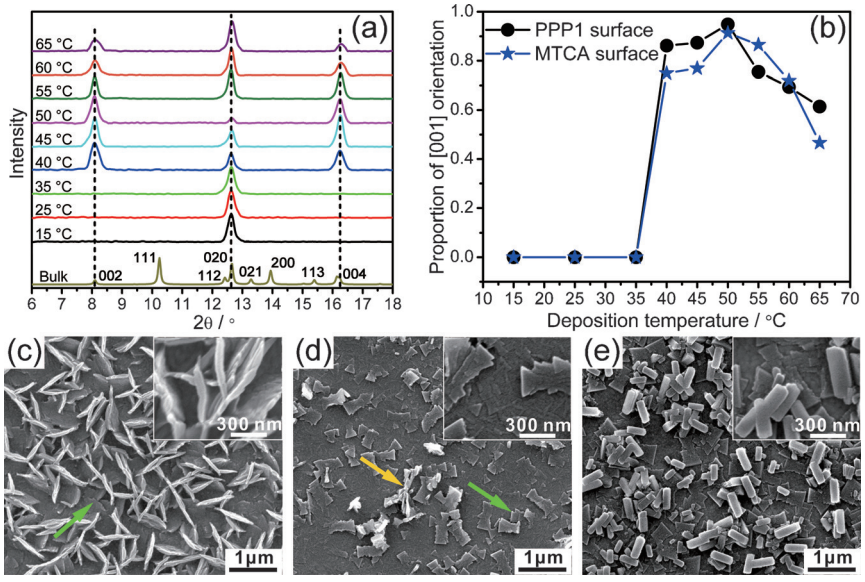

Figure 1. Compilation of the main observations in the growth behavior of the $[Cu_2(sdb)_2(bipy)]$ system. a) Temperature-dependent out-of-plane SXRD data for a 40 cycle SURMOF grown on PPP1. b) Evaluation of the diffraction data for PPP1 and MTCA SAMs. c–e) Scanning electron micrographs of SURMOFs grown for 40 cycles at 15 °C (c), 50 °C (d), and 65 °C (e). The green arrows point out grain boundaries between [001] oriented crystals, while the orange arrow indicates residual [010] oriented crystals protruding from the film.

"bulk" case (40 cycles) between 35 and 40 °C. At first, we suspected that at this temperature a conformational change of the ligand occurs, so that either one or both of the carboxylate groups become rotated with respect to the SO_2 group (in the MOF crystal, the O–O axes of the carboxylate groups and of the sulfone group, respectively, are parallel). This occurrence was excluded by the IR spectra, which showed a slow decay of conformational order in the one-cycle SURMOFs, with increasing temperature (see Figure S6), but no abrupt change at 40 °C. This observation explains the increasing disorder in the third temperature regime ($\tau \geq 55$ °C), but cannot describe the transition between the low- and medium-temperature regimes.

Therefore, we propose that the observed orientational behavior is explained by the interplay of two phenomena, which have been typically disregarded for the growth of SURMOFs, although well recognized in other areas of

surface chemistry: minimization of surface energies and (Ostwald) ripening. A recent publication[36] suggests that the LbL growth follows the Volmer-Weber mechanism, in which the surface growth is not dominated by nucleation but by crystal growth, so that a limited number of crystals form instead of a closed film. In conjunction with the minimization of surface energies, it can be expected that crystals form in a way such that the most energetic surfaces (surface area times surface energy) come into contact with the substrate surface. In case of the orthorhombic $[Cu_2(sdb)_2(bipy)]$ MOF, the (001) surface exposing the highly dipolar SO_2 groups is also the largest crystal face, at least at temperatures below 55 °C (compare Figure 1 c,d). This crystal shape is a result of a slower growth along the [001] direction, in particular in comparison with the one in the [010] direction. Based on these observations, the temperature-dependent behavior of the system can be explained in the following manner: At low temperatures, crystals with different orientation nucleate at the surface, with the [001] ones dominating because of the minimization of surface energy (Figure 3, center left). While this behavior violates the well-established template effects of the groups exposed by the SAMs, different coordinative modes can be imagined in addition to pure van der Waals effects (see Figure S3). Because of the preferred growth in the [001] and [100] direction, the crystals with [001] orientation intergrow, thus effectively blocking their further development (green arrows in Figure 1 and Figure 3). After this, the few crystals with a [001] orientation take up most of the material during the following deposition cycles (Figure 3, lower left), thus leading to the growth of the observed upright platelets (Figure 1 c).

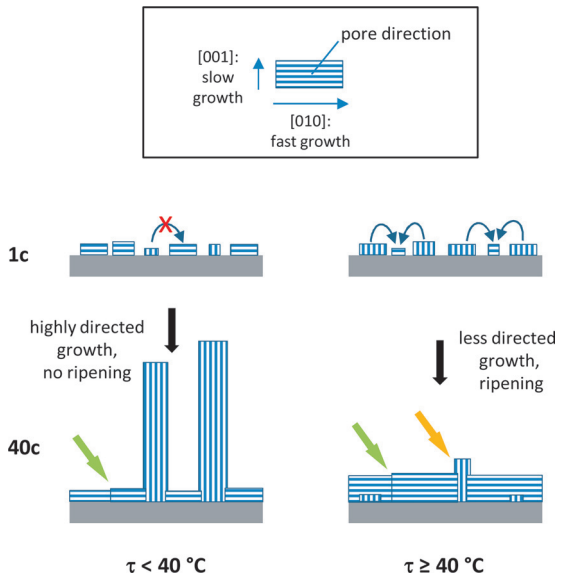

Figure 3. Summary of the observed growth mechanism. In the beginning of the deposition, crystals form in a Volmer–Weber growth mode. While at high temperatures template effects play a role at this phase, at low temperature surface energy minimization predominates. At later growth stages, higher temperatures promote ripening in conjunction with minimization of surface energies leading to reorientation. In contrast, at temperatures below 40 °C, the dominant orientational species is determined by differences in growth rates. The arrows point out the same phenomena as found in Figure 1.

At 40 °C, the crystal lattice energy can be overcome, so that recrystallization (ripening) can occur under the deposition conditions. As has been shown earlier,[31] higher temperatures facilitate the mono-coordination of the apical site of the Cu_2 SBU at the SAM surface, thus promoting nucleation of SURMOFs crystals with [010] orientation. Because of the efficient coordination, these crystals are still flat (Figure 3, center right), but upon further deposition of material it should result in upright plates as in the case of the low-temperature deposits. This large-surface situation is nevertheless supressed by the Ostwald ripening process, which leads to recrystallization during the deposition process and favors the formation of lying-down, [001] oriented crystals (Figure 1 d). Because of the higher temperatures, growth in the [001] direction is less hampered, thus permitting an efficient SURMOF growth.

This hypothesis is supported by micrographs recorded at the different surfaces and different temperatures after deposition of one cycle (see Figure S7). Independent of the surface chemistry and the temperature, all the surfaces show the crystals typical for the Volmer–Weber growth. Regardless of their orientation, all these crystals lie flat on the surfaces with aspect ratios (width/height) between four and ten (see Table S1). The main difference is a higher crystal density in the systems deposited at higher temperatures (55 °C).

In the regime of the highest temperatures, the discrimination between growth velocities is even less pronounced, so that the crystals become less plate-like. This change of shape reduces the differences in the energetic situation, which in conjunction with the increased entropy, as can be seen, for example, by the change of ligand conformation mentioned above, leads to less ordered SURMOF systems.

Regarding the temperature dominance of the different effects, we wanted to make sure that indeed the crystals all have the same quality regardless of their genesis and orientation. While the SXRD data already support similar bulk structures, subtle changes at the surface of the MOFs can influence the growth and also the uptake of guests.[37–39] To test this, the uptake of several guest molecules was determined using a quartz crystal microbalance (QCM). As can be seen in Figure 4, the SURMOFs with a [010] orientation take up almost four times the mass of any guest molecule as compared the ones of the [001] oriented SURMOFs. This behavior can be easily explained by the fact that in the former case the pore openings are exposed towards the ambient, while the respective crystal surfaces of the [001] oriented crystals block each other, as has been discussed above. This distinction can be made by comparing the uptake kinetics of the two systems, which within 1 % are the same (diffusion coefficients of 4.41 and 4.44×10^{-15} $m^2 s^{-1}$ for [010] and [001] orientation, respectively). This data clearly demonstrates that the quality of both the pores and their openings are independent of the orientation, and thus the deposition temperature.

In conclusion, we demonstrated that the growth of scientifically and technologically important SURMOF systems depends on more factors than just the choice of the right

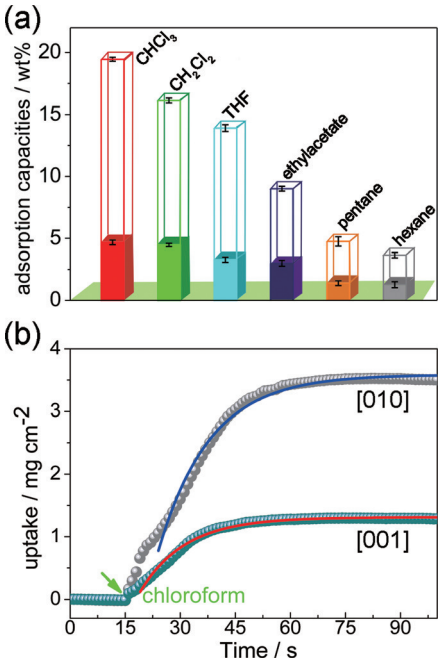

Figure 4. Orientation-dependent absorption properties of the $[Cu_2(sbd)_2(bipy)]$ SURMOF. a) Absolute uptake of different molecules by the [010]-oriented material (empty boxes) and the [001]-oriented SURMOF (filled boxes). The ratio is in all cases about four, thus hinting on inaccessible pores in the [001] case. b) The uptake kinetics for both orientations (here shown for $CHCl_3$, the solid lines are the fit curves to the model) is nevertheless the same, and indicative of similar situations at the pore openings and in the pores. The [010] samples were deposited at 15 °C and the [001] ones at 50 °C.

surface template. In particular temperature-induced ripening processes and the tendency to minimize surface energies can outcompete the template effects. The presented system is insofar unique as it shows a very pronounced temperature onset for the change in crystal orientation, which permitted the analytical dissection of the different influences. These effects (minimization of surface energies, Ostwald ripening) are nevertheless universal and will dominate every liquid epitaxy process, thus explicating why systems with more or less cubic/isotropic crystal shape (such as HKUST-1 and ZIFs) can be grown easily as oriented SURMOFs: here the energy gain by reorienting the crystals is relatively low, so the template effects can dominate the growth. If this interplay of effects is kept in mind, it is nevertheless possible to grow well-oriented SURMOFs even of highly anisotropic systems, as we could show here for the case of $[Cu_2(sdb)_2(bipy)]$.

Experimental Section

For details of the sample preparation and characterization, see the Supporting Information. In short, the layers were grown onto SAM-covered gold surfaces by using a temperature-controlled vessel, in which the substrate was exposed to the following solutions/solvents at different temperatures (15–65 °C): a 1 mM solution of copper acetate dihydrate in ethanol (20 min), 2 × fresh ethanol (5 min), an equimolar H_2(sdb)/bipy mixture (0.1 mM each, 40 min), and 2 × fresh ethanol (5 min). This sequence counts as one cycle. For the absorption measurements, a QCM200 controller (SRS) was used and the SURMOFs were deposited onto SAM-modified QCM25 crystal oscillators (SRS, AT cut, 5 MHz).

Acknowledgments

X.J.Y. is grateful for a Ph.D. fellowship donated by the China Scholarship Council (CSC). Financial support by SKL of Xiamen University of China (No. 201413) and the National Natural Science Foundation of China (No. 21403040) are gratefully acknowledged. We thank Dr. Martin Kind for helpful discussions.

Keywords: adsorption · crystal growth · metal–organic frameworks · surface analysis · surface chemistry

How to cite: *Angew. Chem. Int. Ed.* **2016**, *55*, 8348–8352
Angew. Chem. **2016**, *128*, 8488–8492

[1] A. Bétard, R. A. Fischer, *Chem. Rev.* **2012**, *112*, 1055–1083.
[2] W. J. Li, S. Y. Gao, T. F. Liu, L. W. Han, Z. J. Lin, R. Cao, *Langmuir* **2013**, *29*, 8657–8664.
[3] V. Stavila, A. A. Talin, M. D. Allendorf, *Chem. Soc. Rev.* **2014**, *43*, 5994–6010.
[4] D. Bradshaw, A. Garai, J. Huo, *Chem. Soc. Rev.* **2012**, *41*, 2344–2381.
[5] A. A. Talin, A. Centrone, A. C. Ford, M. E. Foster, V. Stavila, P. Haney, R. A. Kinney, V. Szalai, F. El Gabaly, H. P. Yoon, F. Léonard, M. D. Allendorf, *Science* **2014**, *343*, 66–69.
[6] L. Heinke, M. Tu, S. Wannapaiboon, R. A. Fischer, C. Wöll, *Microporous Mesoporous Mater.* **2015**, *216*, 200–215.
[7] P. Falcaro, R. Ricco, C. M. Doherty, K. Liang, A. J. Hill, M. J. Styles, *Chem. Soc. Rev.* **2014**, *43*, 5513–5560.
[8] S. L. Qiu, M. Xue, G. S. Zhu, *Chem. Soc. Rev.* **2014**, *43*, 6116–6140.
[9] E. Biemmi, C. Scherb, T. Bein, *J. Am. Chem. Soc.* **2007**, *129*, 8054–8055.
[10] Y. S. Li, F. Y. Liang, H. Bux, A. Feldhoff, W. S. Yang, J. Caro, *Angew. Chem. Int. Ed.* **2010**, *49*, 548–551; *Angew. Chem.* **2010**, *122*, 558–561.
[11] R. Ranjan, M. Tsapatsis, *Chem. Mater.* **2009**, *21*, 4920–4924.
[12] O. Shekhah, H. Wang, S. Kowarik, F. Schreiber, M. Paulus, M. Tolan, C. Sternemann, F. Evers, D. Zacher, R. A. Fischer, C. Wöll, *J. Am. Chem. Soc.* **2007**, *129*, 15118–15119.
[13] O. Shekhah, H. Wang, D. Zacher, R. A. Fischer, C. Wöll, *Angew. Chem. Int. Ed.* **2009**, *48*, 5038–5041; *Angew. Chem.* **2009**, *121*, 5138–5142.
[14] A. Schoedel, C. Scherb, T. Bein, *Angew. Chem. Int. Ed.* **2010**, *49*, 7225–7228; *Angew. Chem.* **2010**, *122*, 7383–7386.
[15] M. Tu, R. A. Fischer, *J. Mater. Chem. A* **2014**, *2*, 2018–2022.
[16] V. Stavila, J. Volponi, A. M. Katzenmeyer, M. C. Dixon, M. D. Allendorf, *Chem. Sci.* **2012**, *3*, 1531–1540.
[17] B. Liu, O. Shekhah, H. K. Arslan, J. X. Liu, C. Wöll, R. A. Fischer, *Angew. Chem. Int. Ed.* **2012**, *51*, 807–810; *Angew. Chem.* **2012**, *124*, 831–835.
[18] B. Liu, M. Y. Ma, D. Zacher, A. Bétard, K. Yusenko, N. Metzler-Nolte, C. Wöll, R. A. Fischer, *J. Am. Chem. Soc.* **2011**, *133*, 1734–1737.
[19] N. Nijem, K. Fürsich, S. Kelly, C. Swain, S. R. Leone, M. K. Gilles, *Cryst. Growth Des.* **2015**, *15*, 2948–2957.
[20] J. L. Zhuang, K. Lommel, D. Ceglarek, I. Andrusenko, U. Kolb, S. Maracke, U. Sazama, M. Fröba, A. Terfort, *Chem. Mater.* **2011**, *23*, 5366–5374.
[21] C. Carbonell, I. Imaz, D. Maspoch, *J. Am. Chem. Soc.* **2011**, *133*, 2144–2147.

[22] D. Zacher, K. Yusenko, A. Bétard, S. Henke, M. Molon, T. Ladnorg, O. Shekhah, B. Schüpbach, T. de los Arcos, M. Krasnopolski, M. Meilikhov, J. Winter, A. Terfort, C. Wöll, R. A. Fischer, *Chem. Eur. J.* **2011**, *17*, 1448 – 1455.
[23] M. C. So, S. Y. Jin, H. J. Son, G. P. Wiederrecht, O. K. Farha, J. T. Hupp, *J. Am. Chem. Soc.* **2013**, *135*, 15698 – 15701.
[24] M. E. Silvestre, M. Franzreb, P. G. Weidler, O. Shekhah, C. Wöll, *Adv. Funct. Mater.* **2013**, *23*, 1210 – 1213.
[25] J. L. Zhuang, A. Terfort, C. Wöll, *Coord. Chem. Rev.* **2016**, *307*, 391 – 424.
[26] B. Liu, M. Tu, R. A. Fischer, *Angew. Chem. Int. Ed.* **2013**, *52*, 3402 – 3405; *Angew. Chem.* **2013**, *125*, 3486 – 3489.
[27] Z. B. Wang, H. Sezen, J. X. Liu, C. W. Yang, S. E. Roggenbuck, K. Peikert, M. Fröba, A. Mavrandonakis, B. Supronowicz, T. Heine, H. Gliemann, C. Wöll, *Microporous Mesoporous Mater.* **2015**, *207*, 53 – 60.
[28] J. X. Liu, B. Lukose, O. Shekhah, H. K. Arslan, P. Weidler, H. Gliemann, S. Bräse, S. Grosjean, A. Godt, X. L. Feng, K. Müllen, I. Magdau, T. Heine, C. Wöll, *Sci. Rep.* **2012**, *2*, 921.
[29] Z. B. Wang, J. X. Liu, B. Lukose, Z. G. Gu, P. G. Weidler, H. Gliemann, T. Heine, C. Wöll, *Nano Lett.* **2014**, *14*, 1526 – 1529.
[30] J. X. Liu, O. Shekhah, X. Stammer, H. K. Arslan, B. Liu, B. Schüpbach, A. Terfort, C. Wöll, *Materials* **2012**, *5*, 1581 – 1592.
[31] J. L. Zhuang, M. Kind, C. M. Grytz, F. Farr, M. Diefenbach, S. Tussupbayev, M. C. Holthausen, A. Terfort, *J. Am. Chem. Soc.* **2015**, *137*, 8237 – 8243.
[32] Y. Hijikata, S. Horike, M. Sugimoto, M. Inukai, T. Fukushima, S. Kitagawa, *Inorg. Chem.* **2013**, *52*, 3634 – 3642.
[33] W. J. Zhuang, C. Y. Sun, L. P. Jin, *Polyhedron* **2007**, *26*, 1123 – 1132.
[34] K. Hirai, K. Sumida, M. Meilikhov, N. Louvain, M. Nakahama, H. Uehara, S. Kitagawa, S. Furukawa, *J. Mater. Chem. C* **2014**, *2*, 3336 – 3344.
[35] R. G. Greenler, *J. Chem. Phys.* **1966**, *44*, 310 – 315.
[36] M. L. Ohnsorg, C. K. Beaudoin, M. E. Anderson, *Langmuir* **2015**, *31*, 6114 – 6121.
[37] L. Heinke, Z. G. Gu, C. Wöll, *Nat. Commun.* **2014**, *5*, 4562.
[38] O. Zybaylo, O. Shekhah, H. Wang, M. Tafipolsky, R. Schmid, D. Johannsmann, C. Wöll, *Phys. Chem. Chem. Phys.* **2010**, *12*, 8092 – 8098.
[39] L. Heinke, C. Wöll, *Phys. Chem. Chem. Phys.* **2013**, *15*, 9295 – 9299.

Received: March 23, 2016
Published online: June 3, 2016

